Behavior of tunnel form buildings under quasi-static cyclic lateral loading

S. Bahadir Yuksel†

Selcuk University, Department of Civil Engineering, Konya 42075, Turkey

Erol Kalkan‡

California Geological Survey, Earthquake Engineering Program, Sacramento, 95814 CA

(Received , 2006, Accepted , 2006)

Abstract. In this paper, experimental investigations on the inelastic seismic behavior of tunnel form buildings (i.e., box-type or panel systems) are presented. Two four-story scaled building specimens were tested under quasi-static cyclic lateral loading in longitudinal and transverse directions. The experimental results and supplemental finite element simulations collectively indicate that lightly reinforced structural walls of tunnel form buildings may exhibit brittle flexural failure under seismic action. The global tension/compression couple triggers this failure mechanism by creating pure axial tension in outermost shear-walls. This type of failure takes place due to rupturing of longitudinal reinforcement without crushing of concrete, therefore is of particular interest in emphasizing the mode of failure that is not routinely considered during seismic design of shear-wall dominant structural systems.

Keywords: Reinforced concrete; shear-wall; brittle failure; tunnel form building; box system; cyclic loading; finite elements.

1. Introduction

Tunnel form buildings are primary housing of many countries due to their industrialized modular construction technique where in-situ concrete is poured into two half-tunnel forms to shape load-bearing walls (shear-walls) and floor slabs simultaneously. When this process is repeated, generally in a 24-hour cycle per floor, residential units can be rapidly built up. That makes tunnel form construction system an attractive proposition for the erection of medium to high-rise buildings having repetitive elements or layouts. A typical tunnel form building in construction stage is demonstrated in Fig. 1. In this figure, left panels illustrate the half tunnel shape formwork system (so called "tunnel form unit"), and typical openings in a shear-wall and their reinforcing detailing. The right panel in Fig. 1 exhibits the precast façade walls and also sliding form unit generally used to construct the corners of tunnel form buildings and the interior shafts (e.g., elevator shafts and/or stair cases). Tunnel form buildings diverge from other conventional reinforced concrete (RC)

†

‡ Corresponding author, E-mail: Erol.Kalkan@conservation.ca.gov

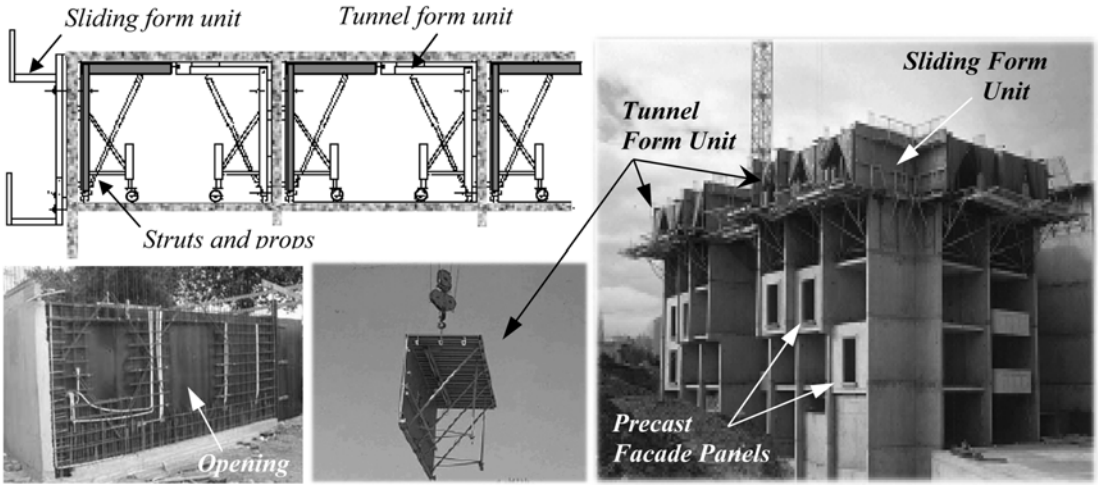

Fig. 1 Elements of tunnel form system (i.e., sliding form unit and tunnel form unit) with typical opening in shear-wall (*left three panels*); tunnel form building in construction stage (*right panel*)

structures due to lack of beams and columns in their structural integrity. In these buildings, all the vertical load-carrying members are made of shear-walls, and floor system is flat plate. Both gravity and lateral loads (seismic or wind) are transferred to shear-walls. Non-structural components such as façade walls, stairs, landings and partition walls are used as prefabricated elements to expedite the construction process.

Recent studies (Lee *et al.* 2004; Balkaya and Kalkan 2003, 2004; Ghrib and Mamedov 2004) show that current seismic codes and design provisions (e.g., IBC 2000, UBC 1997, TSC 1998) inaccurately estimates the period and response-modification-factor for tunnel form buildings despite the fact that these parameters are directly used to compute the design base shear. In addition, there is a lack of experimental work to understand the three-dimensional (3D) response of tunnel form buildings under extreme lateral loading conditions. Previous experimental studies conducted on shear-wall systems were generally limited to two-dimensional (2D) investigations. However, it was analytically proven that the 2D approach is not adequate to capture important behavior of tunnel form buildings under seismic action due to significant slab-wall interaction and global tension-compression (T/C) coupling effects (Balkaya and Kalkan 2003, 2004).

This paper reports an experimental program in which quasi-static cyclic testing of two four-story 1/5-scale tunnel form buildings were conducted (Yuksel 2003). Results of this study will augment the literature with the tests involving 3D wall configurations where the response is dominated by flexure triggered brittle mechanism. This failure mechanism is similar to that observed in an eight-story heavily damaged shear-wall dominant building (El-Faro building) during the 1985 Chile earthquake (Wood *et al.* 1991), therefore is of particular interest in emphasizing the mode of failure that is not routinely considered during seismic design of shear-wall dominant structural systems.

2. Research significance

Previous investigations (Lee *et al.* 2004, Balkaya and Kalkan 2003, 2004, Ghrib and Mamedov

2004) indicated some deficiencies in design codes to provide adequate guidelines for the primary seismic design parameters (such as period estimates and response modification factor (R)) of tunnel form buildings. This paper, in part, sheds light on some important behavioral issues by examining the results of a test program in which four-story scaled tunnel form building specimens were tested under quasi-static cyclic lateral loading. Results of this study supplemented by finite element simulations indicate that structural walls of tunnel form buildings may exhibit brittle flexural failure under lateral loading. The global tension/compression couple triggers this failure mechanism by creating pure axial tension in outermost shear-walls.

Fig. 2 Test specimens

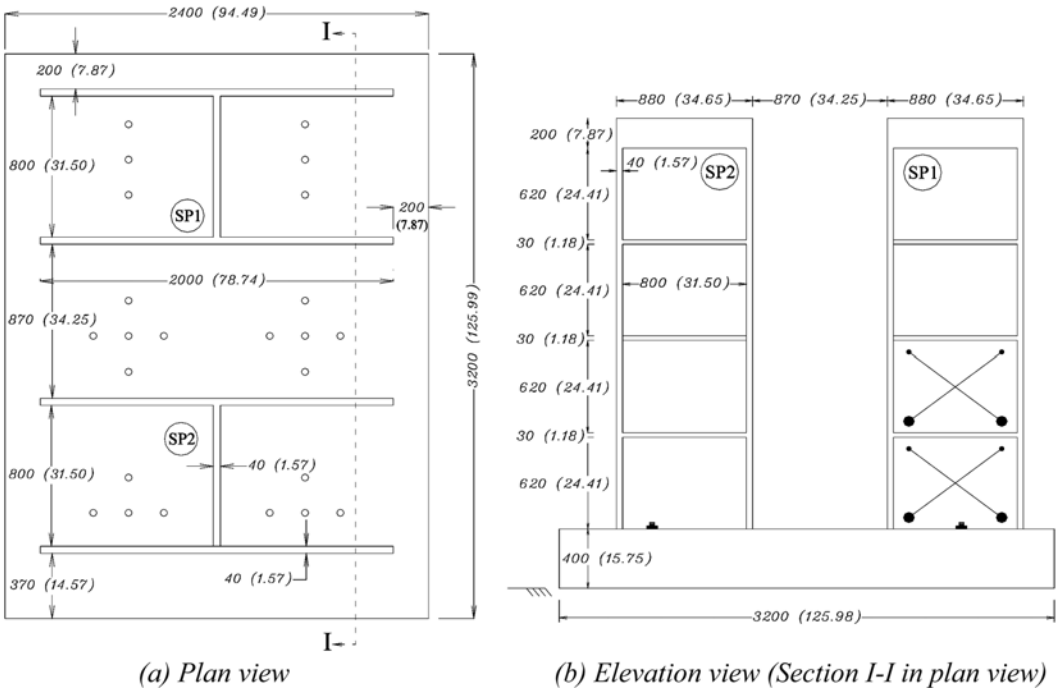

(a) Plan view *(b) Elevation view (Section I-I in plan view)*

Fig. 3 (a) Plan view, (b) Elevation view of the test specimens, *units are in mm (inch)*

3. Experimental procedure

The experimental work described herein involves the testing of two four-story 1/5-scale RC tunnel form building test specimens as shown in Fig. 2. The specimens are the representatives of a typical tunnel form section in a regular tunnel form building. Fig. 3 exhibits their plan and elevation views. Both specimens had identical dimensions, reinforcement detailing and material properties. Testing program consisted of lateral cyclic lateral loading. The specimen tested along its weak axis is referred as SP1, and the other specimen tested along its strong axis is called as SP2. This study attempted to make the material properties and reinforcement detailing of scaled models identical to those utilized in conventional tunnel form building constructions in Turkey. Thus, the material size used in specimens, such as maximum size of aggregates, diameter and spacing of the reinforcement were reduced to account for the scaling effects. Mass scaling was not performed due to applied static loading where the inertial effects become negligible.

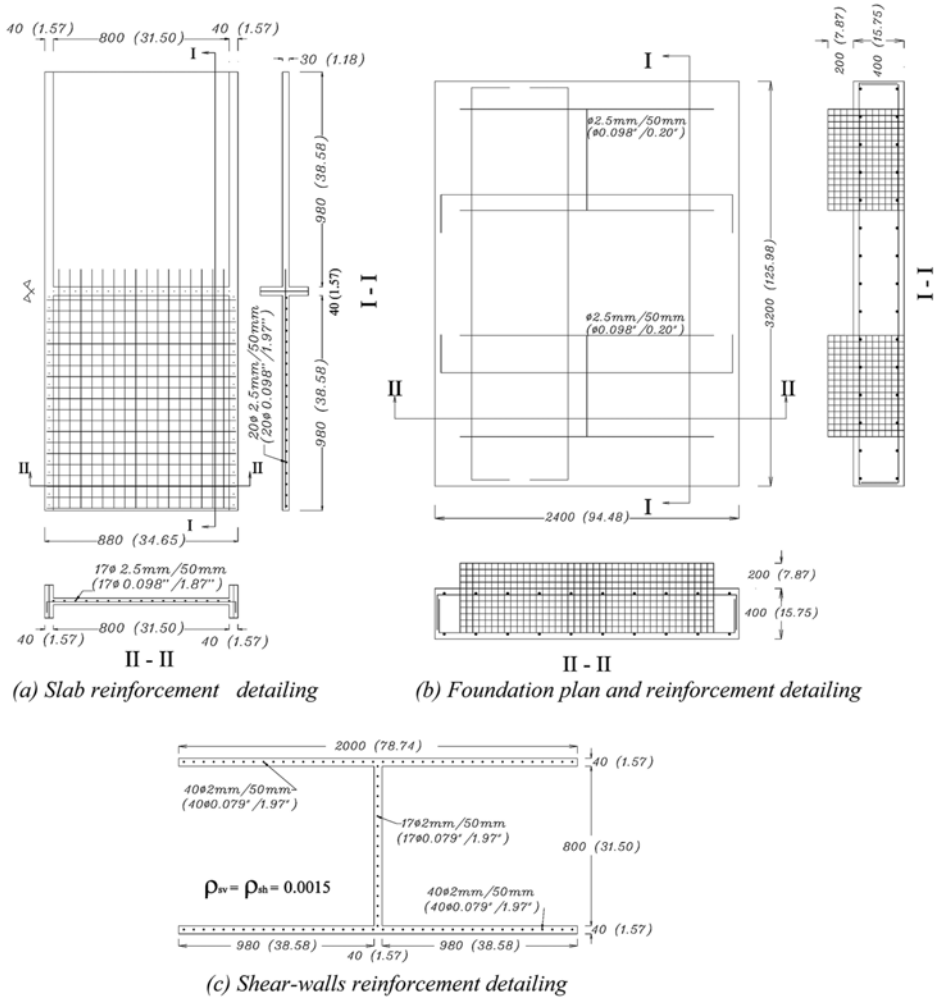

Fig. 4 Reinforcement detailing of specimens, SP1 and SP2: (a) Slab, (b) Foundation, (c) Shear-walls, *units are in mm (inch)*

Table 1 Material properties of reinforcement steel

Location	Diameter		f_{sy}		f_{su}		ε_{sy} ($\times 10^{-3}$)	ε_{su} ($\times 10^{-2}$)
	mm	inch	Mpa	ksi	Mpa	ksi		
Shear-wall	2.0	0.08	540	78.3	600	87.0	2.7	2.5
Slab & Foundation	2.5	0.10	540	78.3	600	87.0	2.7	2.5

3.1 Details of test specimens

Both specimens were monolithically constructed at each floor level similar to standard applications. They were manufactured on the same foundation, clamped to the strong floor by high-strength steel bolts. The reinforcement detailing of foundation of the test specimens as well as those of slabs and shear-walls are presented in Fig. 4. It should be noted that the walls in the longitudinal direction are referred as flange walls and the walls in the short direction are referred as web walls. The amount of reinforcement used in the walls corresponded to minimum vertical and horizontal reinforcement ratio (i.e., ratio of reinforcement area to gross concrete area) requirement (ρ_{sv}, ρ_{sh} = 0.0015) of the regulatory seismic design code in Turkey (TSC 1998). Mesh reinforcement for the walls consisted of 2 mm (0.08") diameter plain bars. Such small diameter bars are not commercially available. They were manufactured by drawing out larger diameter bars to replicate the same procedure applied for commercially available mesh reinforcement used in practice. This process normally leads cold worked steel. It should be also noted that mesh reinforcement used in shear-walls of tunnel form buildings have relatively small diameter bars (5.0 mm, 5.5 mm, etc.) compared to those used in conventional shear-walls of RC buildings. Additional tensile tests were conducted on reduced diameter reinforcing bars to assure a realistic behavior of reinforcing bars.

As shown in Fig. 4, single-layer mesh reinforcement was placed in the middle of the walls. Bar spacing in the vertical and horizontal directions were kept 50 mm (1.97"). The wall reinforcement was spliced at floor levels with a splice length of 50 bar diameters (100 mm, 3.94"). The longitudinal reinforcement of the first story walls was spliced at 100 bar diameters (200 mm, 7.87") at foundation level. To transmit the load from the superstructure to the foundation, 2.5 mm (0.1") diameter mesh reinforcements with 50 × 50 mm (1.97" × 1.97") spacing were used as dowels. To provide adequate development length, these dowels were extended into the footing by 300 mm (11.81") and tied to the foundation reinforcement. In slabs, 2.5 mm (0.1") diameter single-layer mesh reinforcement located in the middle of the section was used at a spacing of 50 mm (1.97") in both horizontal directions. The ends of the bars had an anchorage length of 50 mm (1.97") in the form of a 90-degree bend. Different than the wall reinforcement ratio, the ratio of slab reinforcement along each orthogonal direction was 0.0025. The material properties of reinforcing steel are provided in Table 1. The concrete strength of the test specimens was 35 MPa (5.08 ksi) on the day of testing. The ultimate strength values of reinforcement and concrete used in the test specimens are in compliance with those used in practice.

3.2 Instrumentation and test procedure

The testing system consisted of strong floor, reaction wall, loading equipment, instrumentation and data acquisition system (see Fig. 2). The lateral loading system consisted of a load cell (110 kN (24.7 kips) compression-tension), hydraulic jack and hinges at the ends. Strain gage-based linear variable

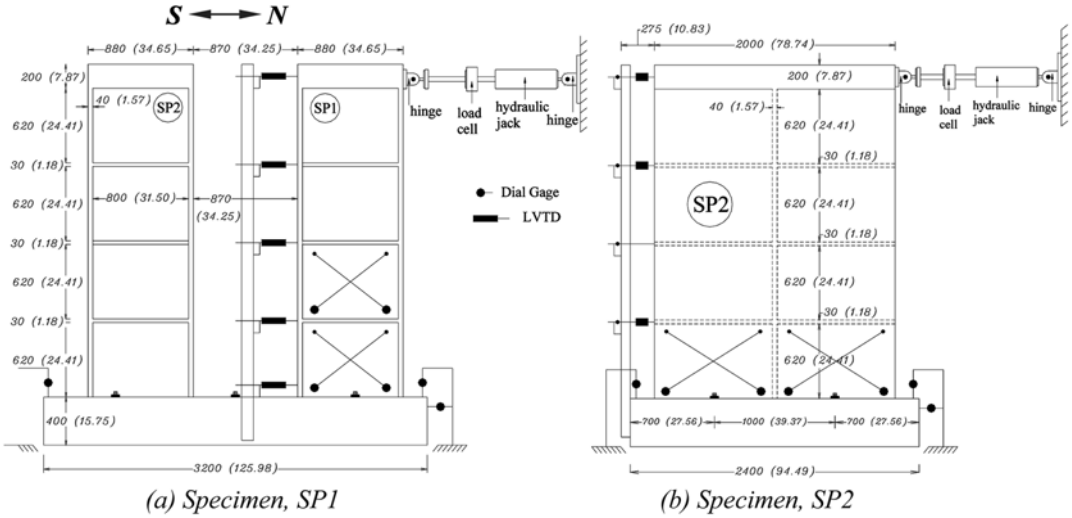

Fig. 5 Test setup, loading system and instrumentation, *units are in mm (inch)*

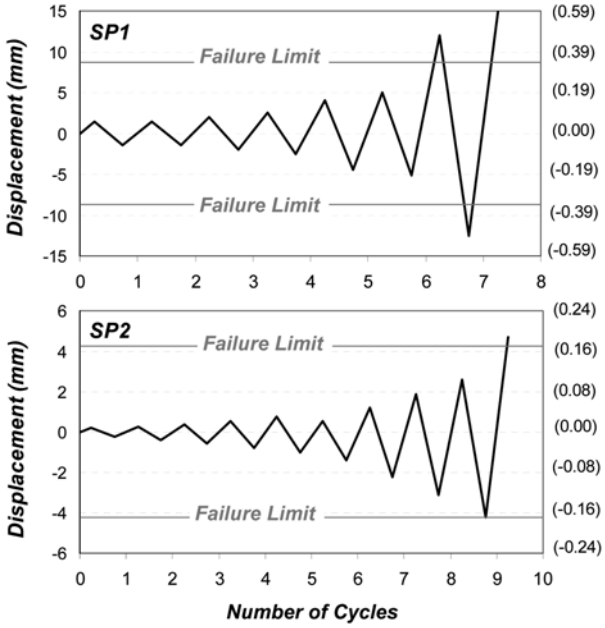

Fig. 6 Quasi-static cyclic loading history, *units are in mm (inch)*

differential transformers (LVDTs) and dial gages (DGs) were used to measure the displacements. Additionally, the lateral displacements at each story level were measured by displacement transducers. Average shear deformations of the walls were measured by diagonally placed displacement transducers. Details of the instrumentation and test-setup are demonstrated in Fig. 5.

The specimens were subjected to quasi-static cyclic lateral loading. The loading history in terms of number of cycles versus roof displacement is presented in Fig. 6. Loading the specimens to a predetermined level and then unloading to zero level constituted a half-cycle.

4. Test results

For SP1, the flange close to the reaction wall is henceforth called as north flange and the flange away from the reaction wall is called as south flange (see Fig. 5(a) for north and south directions). For SP1, the maximum top displacement of 8.7 mm (0.34”) was recorded under 40 kN (9 kips) lateral load. During the loading process, the horizontal flexural cracks initiated at the outer surface and boundaries of the flanges and propagated towards the center of the flanges. At the 17 kN (3.82 kips) lateral load level of the first positive half cycle (positive cycle refers to pushing of the specimen against the laboratory reaction wall), a minor visible hair crack initiated at the first story slab wall connection at the left side of the north flange. When the first two cycles were completed, this crack length reached to 740 mm (29.1”) and surfaced approximately 650 mm (25.6”) above the foundation. The same crack pattern was observed at the end of the second cycle and located at the right side of the south flange at the first story slab wall connection with a crack length of 440 mm (17.3”). This crack also appeared at 650 mm (25.6”) above the foundation. A horizontal flexural crack mobilized at the foundation wall joint at the north face in the third cycle. During the fourth excursion, lateral load was increased to 30 kN (6.74 kips). At the fourth positive cycle, flange cracks located at the slab wall joint of the north flange of first story propagated from the right edge to the center of the flange and another horizontal crack initiated at the left edge and propagated towards the center of the flange wall. In the fourth negative cycle, a new horizontal crack started to initiate at the right edge of the south flange at the first story slab wall connection. During that cycle, another crack at the second story slab wall connection started to initiate at the right side of the south flange. It was 330 mm (13”) in length and located approximately 1300 mm (51.2”) above the foundation. At the fifth positive cycle (when the lateral load reached to 35 kN (7.9 kips)), the lateral load suddenly dropped to 30 kN (6.74 kips) due to brittle tension crack surfaced across the entire length of the north flange at 380 mm (15”) above the foundation (see Fig. 7(a)). At this cycle, an inclined crack appeared on the web and it was identical at both sides of the wall (Fig. 7(c)). Similar phenomenon raised on the south flange during the negative cycle. As such, 35 kN (7.9 kips) lateral load resulted in tension crack traveling horizontally along the length of the flange. It was again a horizontal flexural crack formed 400 mm (15.75”) above the foundation (Fig. 7(b)). These horizontal flexural cracks at the flanges occurred in a very sudden and brittle manner.

Following the positive sixth cycle, new shear cracks (inclined 45 degrees from the horizontal) developed at the web wall and a new horizontal flange crack occurred 200 mm (7.87”) above the foundation at the south flange (Fig. 7(d)). At the end of this cycle, this horizontal crack ran along the entire south flange. At the seventh positive cycle, a new horizontal flexural crack at the north flange formed 490 mm (18.9”) above the foundation when the horizontal lateral load exceeded 35 kN (7.9 kips). When the lateral load reached 40 kN (9 kips), all the horizontal reinforcement ruptured suddenly 380 mm (15”) above the foundation level at the north flange. The same behavior was also observed at the south flange during the seventh negative cycle. When the horizontal lateral load exceeded –35 kN (–7.9 kips), a horizontal flexural crack occurred 420 mm (16.5”) above the foundation level at the south flange. This horizontal flange crack (480 mm (18.9”) in length) occurred at the right edge of the south flange and propagated towards the center. When the lateral load reached –40 kN (–9 kips), all the reinforcement in the south flange ruptured at 380 mm (14.96”) above the foundation suddenly similar to the north flange (Fig. 7(e),(f)). By the end of testing SP1, three major flexural cracks (extended the full width and thickness of the flange) spaced

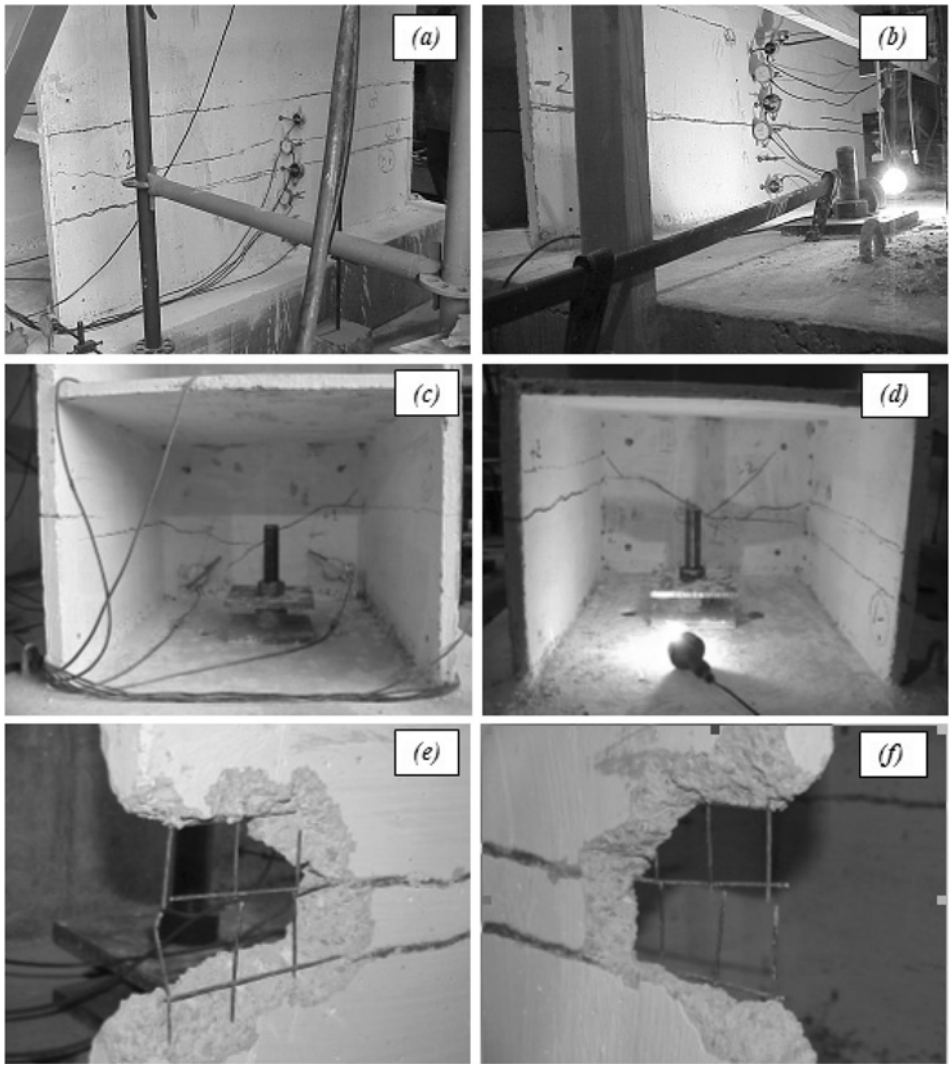

Fig. 7 Crack initiation and propagation in specimen SP1

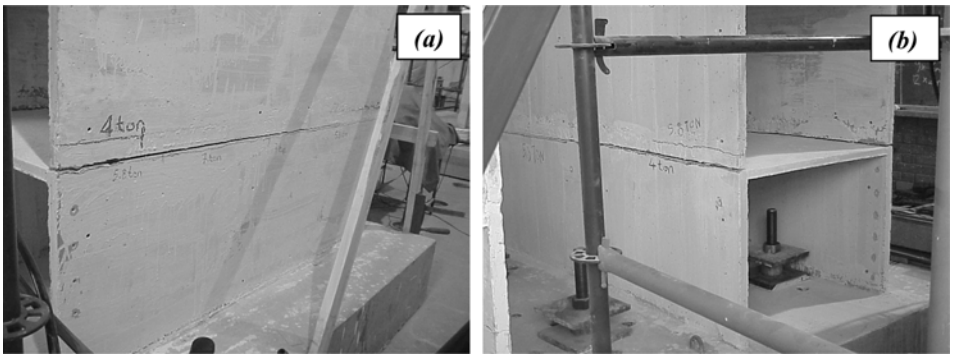

Fig. 8 Crack propagation along first story slab wall connection of specimen SP2 after the last positive cycle

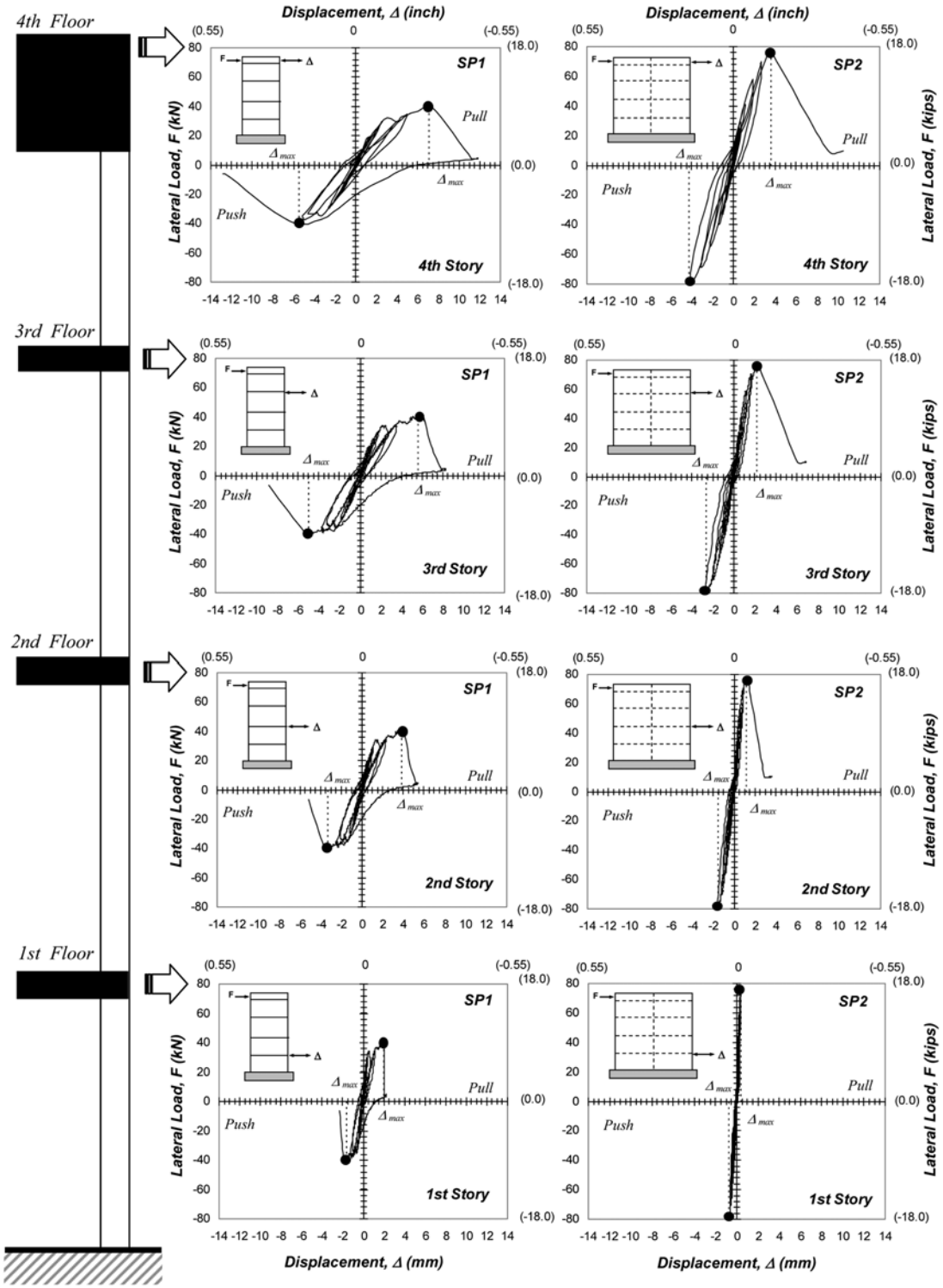

Fig. 9 Lateral load-displacement response at each story level for specimens, SP1 and SP2

along the height of the first story were evident, yet no cracks were observed on the second, third and fourth story walls with lone exception of slab wall joint crack at the second story. Crushing of the concrete was not observed during the quasi-static testing of SP1.

For SP2, the maximum lateral load was measured as 80 kN (18 kips). Maximum lateral displacement was 4.3 mm (0.17") at the roof level. During the second positive cycle, lateral load was increased to 15 kN (3.4 kips) that initiated the first visible cracks (horizontal flexural hairline cracks) located at the foundation wall joint of both flanges at the tension side. At the fourth cycle, 25 kN (5.6 kips) lateral load was applied. When the fourth cycle was completed, the horizontal foundation wall cracks propagated towards the center in both faces of the specimen. At the fifth positive cycle, as the lateral load was pointed to 25 kN (5.6 kips), a sudden tension crack at the first story slab wall construction joint formed and the lateral load stayed constant, then lateral load was increased up to 30 kN (6.7 kips). This flexural crack first initiated at the slab wall construction joint at the tension side then propagated towards the center. At the negative excursion, a similar crack formed at the tension side and propagated through the neutral axis. At the seventh cycle, a lateral load of 60 kN (13.4 kips) was applied. That force resulted in a new horizontal crack at the second story slab wall construction joint. Lateral load was further increased to 80 kN (18 kips) at the last cycle and this load level caused a sudden rupture of reinforcement at the first-story slab wall construction joint at the tension side (Fig. 8). During the negative excursion (–80 kN, –18 kips), all the reinforcement at the other side ruptured.

For SP2, cracking patterns in the flanges were horizontal and essentially identical at the end of each cycle. Similar to SP1, flange cracks propagated from the boundaries of the flanges towards the center of the flanges. Shear cracks and crushing of the concrete were not observed in the testing of SP2. The major crack was the first story wall-slab construction joint crack at the flange walls. Fig. 9 demonstrates the individual load-deformation response at each story level for both specimens. Although the load-displacement results for SP1 and SP2 were different, their ultimate capacity was controlled by the low reinforcement ratio of the walls. In general, the unloading curves of the second excursion at each displacement level followed the same trend as the first. Compared to the SP1, the specimen SP2 exhibited more rigid behavior and was able to carry higher lateral load with less deformation at each story level.

5. Brittle failure mechanism of tunnel form buildings

For specimens SP1 and SP2, the mode of the failure was brittle. The crushing of concrete was not observed and the damage was concentrated on the shear-walls only. This failure mechanism occurred due to low longitudinal reinforcement ratio of walls and negative contribution of low axial load viz, section cracked as a consequence of tensile forces acting opposite direction of axial load. In other words, low axial load has less contribution in retarding the tensile stress initiation. As soon as the tensile stress in the concrete exceeded the modulus of rupture (tensile strength), the cracking took place and the concrete immediately released the tensile force it carried. Then, the lightly stressed steel absorbed this increment of load. For both specimens, the minimum amount of longitudinal steel was unable to carry the additional load, therefore following the cracking of concrete, longitudinal reinforcements yielded and ruptured suddenly without warning. The damage in SP2 was concentrated on the first-story slab wall connection, potentially a zone of weakness due to the construction joint.

The observed damage conditions of the test specimens were investigated based on two vulnerability indexes so called "shear-stress-index" and "flexural-stress-index". These indexes were originally proposed by Wood (1989, 1990) to determine the vulnerability of a wall to the fracture of the reinforcement. The shear-stress index (v_{max}/v_n) was first introduced to distinguish between the shear and flexural modes of failure. In the definition of the shear-stress index, v_n stands for the nominal shear-strength defined according to ACI 318-83 (1983) as

$$v_n = \alpha_c \sqrt{f_c'} + \rho_n f_y \tag{1}$$

where α_c changes from 3.0 for walls having an aspect ratio (h_w/l_w) less than 1.5 to 2.0 for walls with an aspect ratio greater than 2.0. v_{max} denotes the maximum average shear-stress (i.e., V_{max}/A_{cv}). According to experimental study of Wood (1989), of the 13 walls that developed a shear-stress index less than 0.75, 12 failed in flexure. For specimens SP1 and SP2 (both failed in flexure) shear-stress indexes were found to be 0.63 and 0.28 being less than the limiting value of 0.75.

Among flexural failures, steel strain in the extreme layer of reinforcement at the nominal flexural capacity of the cross section was used by Wood (1989) as the second index for the walls that are susceptible to fracture of longitudinal reinforcement. This flexural-stress-index was defined as ($\rho_t f_y + P/A)/f_c'$. According to the test results reported in Wood (1989), failures due to the fracture of the reinforcement were observed in walls with flexural-stress ratio less than 15 percent. For SP1 and SP2, flexural stress ratio was computed as 2.7 percent, which is much less than the limiting value of 15 percent. The computed low values of shear-stress-index and flexural-stress-index for SP1 and SP2 were found to be in agreement with the previous experimental observations, and served as explicit indicators of the reinforcement rupture triggered failure mechanism.

Similar failure mechanism of structural walls was also reported in the literature. The investigations on 37 laboratory tests of structural walls, Wood (1991, 1989) showed that the flexural capacity of most walls with total reinforcement ratios less than 0.01 was limited by the fracture of the longitudinal reinforcement. Similar to our experimental findings, in two of the lightly reinforced walls investigated by Wood (1991, 1989), the longitudinal reinforcement fractured before crushing of concrete. In order to prevent such failure mechanism in flexural members, ACI 318-02 (2002) requires that beam members should be reinforced with an area of steel in both positive and negative moment regions not less than $3(b_w \cdot d)\sqrt{f_c'}/f_y$ and $200(b_w \cdot d)/f_y$ (in English unit system) to ensure that the nominal flexural strength will exceed the cracking moment by a safe margin. Different than requirements for beam members, for structural walls, ACI 318-02 (2002) places 0.0012 or 0.0015 limits (depends on the bar size and reinforcement yield strength) as the ratio of vertical reinforcement area to gross concrete area. The failure of two test specimens having vertical reinforcement ratio of 0.0015 questions the adequacy of the minimum vertical reinforcement to prevent the brittle failure.

6. Three-dimensional tension/compression coupling

Due to wall-configurations in plan of tunnel form buildings, in-plane or membrane forces in shear-walls result in tension-compression (T/C) force couple associated with combined effects of wall-to-wall (even including walls with openings) and wall-to-slab interactions (Balkaya and Kalkan 2004). In this mechanism, the outer walls oriented perpendicular to lateral loading direction, act as

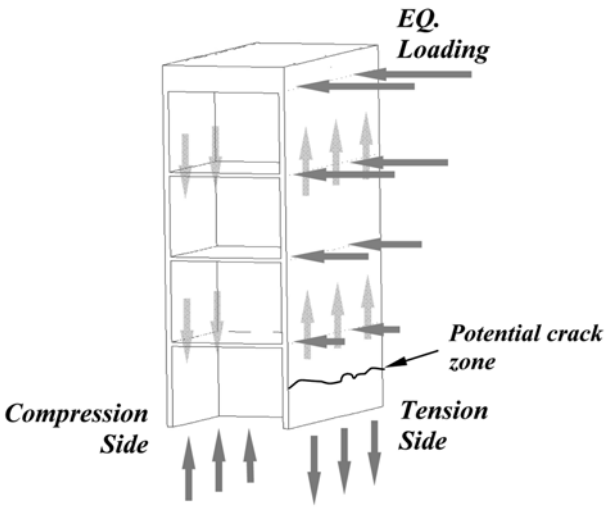

Fig. 10 Global tension-compression (T/C) force couple in a typical tunnel form section

flanges when subjected to bending loads and resist against total moment primarily in tension and compression. Whereas, the inner walls passing from the centroid and oriented to the same direction with lateral loading act in bending and their contribution to overall moment capacity are relatively small. In general, this 3D originated mechanism shows a characteristic T-section behavior. Therefore, the resultant force mechanism exhibits a significant contribution to the capacity and seismic performance of buildings. The typical T/C coupling mechanism in tunnel form building section is illustrated in Fig. 10.

Tunnel form buildings diverge from classical frame and shear-wall-frame structures by providing significantly larger cross section area to carry the vertical loads. That turns axial stress ratio $N/(f_c' \cdot A_g)$ remarkably smaller and less significant compared to those for structural components of conventional RC buildings. Due to global T/C behavior, axial load in shear-walls at the tension side may become zero or even negative during seismic action. As the height of the building becomes larger than the plan dimension in the direction of loading, the global T/C effects exacerbate. In this condition, pure axial tension may develop and cause longitudinal tension cracks followed by sudden tensile loading carried by the wall reinforcements only. If the wall reinforcements were not adequately quantified and detailed, this tensile load would result in sudden failure of the wall without warning.

7. Computer simulations

The behavior of test specimens under lateral loading was also numerically simulated through three-dimensional (3D) finite element (FE) models created using the general-purpose nonlinear finite element program TNO-DIANA (2004). The eight-noded brick element having a four-by-four gauss integration points were utilized in more than 13000 elements for modeling walls and slabs. In analytical models, the governing nonlinear phenomena in the ultimate limit state were cracking and crushing of concrete and plastic behavior of reinforcement steel. The applied analysis procedure was

based on the total strain cracking model (cracks have opening/closing and rotating capabilities) using secant-stiffness approach. The compression behavior of concrete was modeled using unconfined concrete model proposed by Popovics (1973) and modified by Thorenfeldt *et al*. (1987). The tension stiffening of concrete was considered as linear ascending curve up to cracking limit, and tension softening portion of stress-strain curve was based on the model proposed by Hordijk (1991), which utilizes mode-I fracture energy, ultimate tensile strength and crack bandwidth to compute the maximum crack opening. The approximated concrete stress-strain relationship in compression and tension is shown respectively in Figs. 11(a) and 11(b). Constant shear retention factor (β-factor) to account for the degradation in the modulus of rigidity after crack initiation was utilized as 0.1 (Fig. 11(c)). Poison's ratio for concrete was approximated as 0.20 based on the verification studies.

The constitutive behavior of the reinforcing steel was modeled by Von-Mises plasticity model with an associated flow law and isotropic strain hardening. Smeared reinforcement model, treated as an equivalent uniaxial layer of the material at the appropriate depth and smeared out over the element as several orthotropic layers, was utilized to simulate the reinforcement mesh. Transferring the strength and stiffness of the reinforcement directly into the concrete elements, this model is the easiest to implement the modeling of mesh-reinforcement (Balkaya and Kalkan 2003). Perfect bond was assumed and steel nodes were rigidly attached to concrete element nodes. The material properties and stress-strain relationship of the reinforcing steel used are presented in Fig. 11(d). Further details of FE models can be found in Kalkan and Yuksel (2007).

Nonlinear static pushover analyses were applied whereby the FE models were pushed laterally with incrementally increasing lateral displacement from the roof level. Displacement control

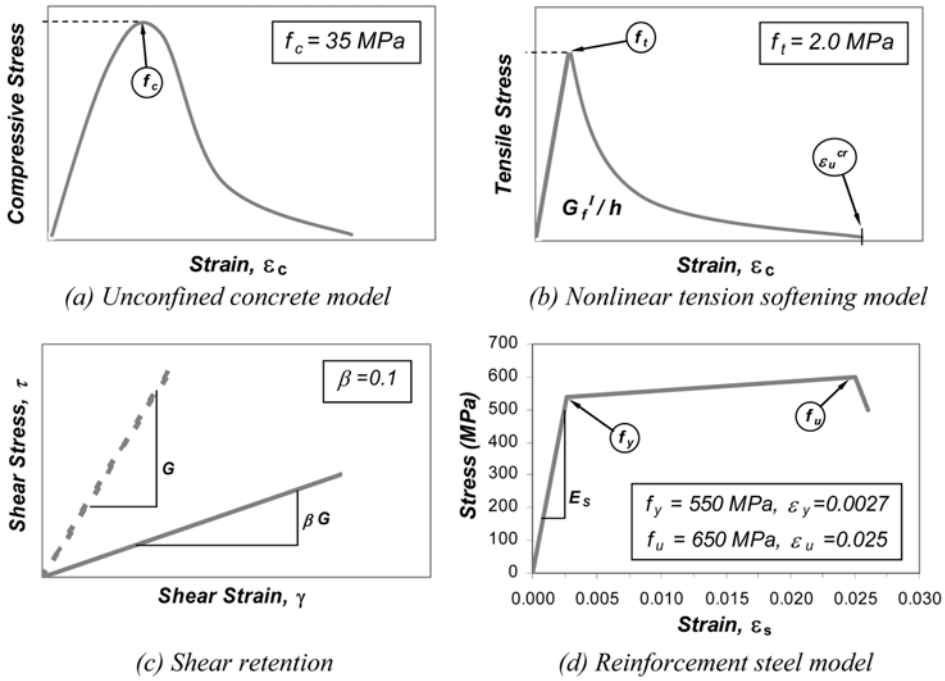

Fig. 11 Concrete and steel nonlinear material models

analyses were conducted in two horizontal directions separately (corresponding to similar loading directions of the test specimens) while the gravity load was kept sustained. Based on the analyses, load-deflection curves were obtained for both specimens and compared to envelope curves produced from experimental results in Fig. 12. The envelope curves contain the maximum loads at each displacement level. Experimentally obtained plots show that the lateral load carrying capacity of SP2 (loaded along strong-axis) is two times larger than that of SP1 (loaded along weak-axis). Conversely, SP1 provided maximum lateral displacement two times larger than that of SP2. Compared to experimental results, the computed response of FE models is somewhat stiffer and stronger. Some of the discrepancy can be attributed to complex three-dimensional behavior and primarily the difference between monotonically increasing loading and cyclic loading, but some is also due to modeling assumptions (e.g., perfect bond assumption for reinforcing steel). Despite these discrepancies, comparison of results reveals that the analytical models reasonably captured the salient response characteristics of the test specimens.

More importantly, the FE models provide approximately similar cracking patterns observed in the experiments as depicted in Fig. 13. Figs. 13(a) and 13(b) clearly manifest the high stress concentration when the model is loaded along its weak axis (as in SP1) and yielding of longitudinal reinforcement as well as mobilization of horizontal cracking above the mid-height of the first story flanges of SP1. Similar to experimental observations, diagonal cracking occurred on the web wall in the analytical model. The loading of the FE model along the strong axis (as in SP2) resulted in reasonably similar damage pattern observed experimentally. To be more specific, the yielding of steel (Fig. 13(c)) and cracking of concrete concentrated on the first story slab wall connection joint (Fig 13(d)).

These comparisons show the capability of the computer model. This model was later used to investigate the amount of minimum steel area and essential reinforcement detailing to prevent brittle failure of tunnel form buildings by providing sufficient ductility and energy dissipation capacity in a series of parametric study reported in Kalkan and Yuksel (2007).

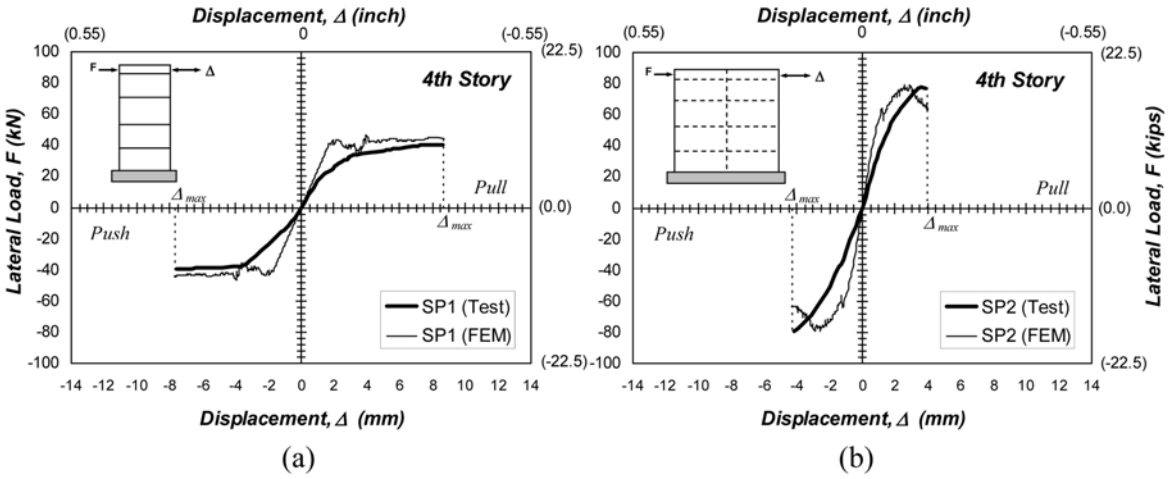

Fig. 12 Computed capacity curves and experimental cyclic envelope curves: (a) Specimen SP1, (b) Specimen SP2

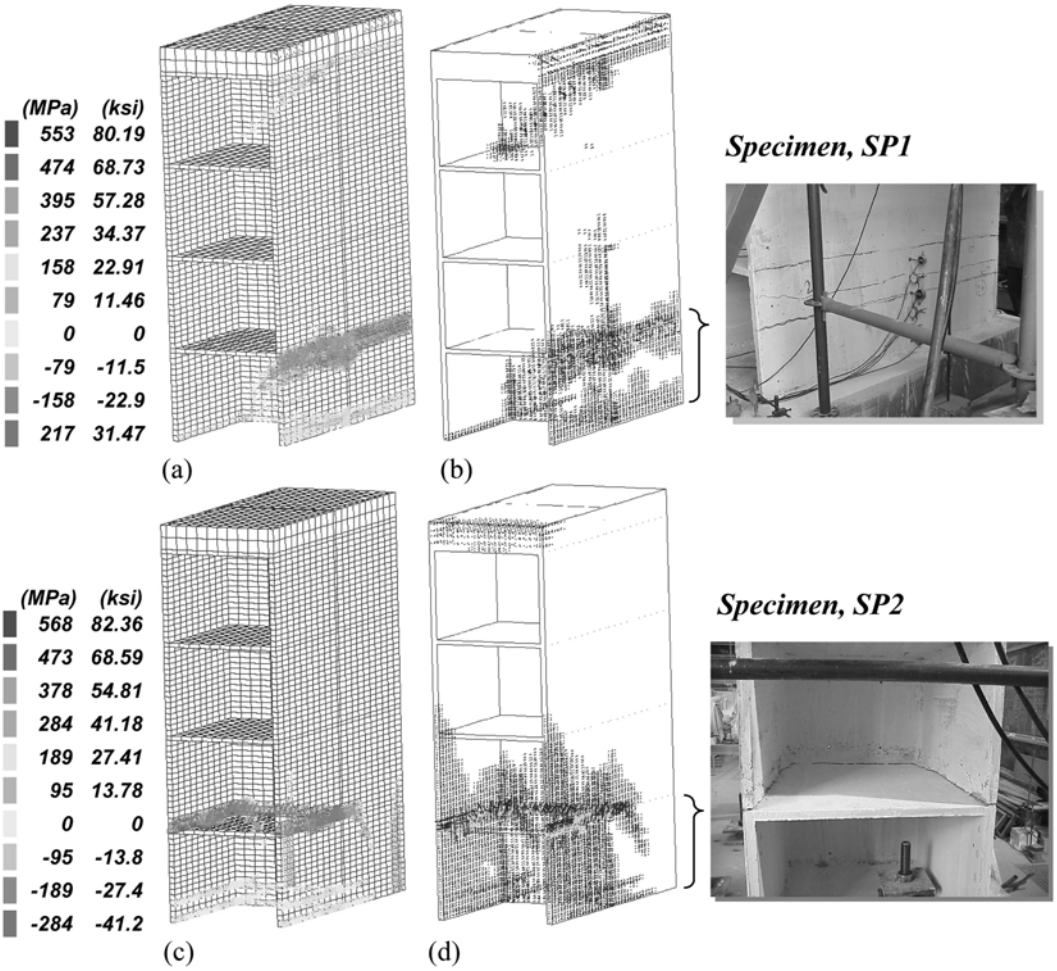

Fig. 13 (a,c) Stress concentration on longitudinal bars at failure (*Note: Yield strength of steel is 540 MPa (78 ksi), negative sign indicates compression*), (b,d) Experimental and analytical damage patterns

8. Conclusions

In this paper, three-dimensional behavior of tunnel form buildings under loading to failure is investigated. Two scaled specimens were tested under quasi-static-cyclic lateral loading. The test specimens were purposely detailed and constructed to reflect the common practice in Turkey, thereby minimum amount of mesh reinforcement was used in shear-walls. Experimental and analytical findings of the study show that brittle flexural failure may take place in tunnel form buildings due to fracture of longitudinal reinforcement in shear-walls. This failure mechanism, also observed in finite element simulations, is triggered as a result of low reinforcement ratio with a negative contribution of low axial load, which eventually controls the level of bending moment for the crack initiation. Similar failure condition was observed in the eight-story shear-wall dominant building (El Faro building) during the 1985 Chile earthquake. This building sustained severe structural damage after the longitudinal reinforcement fractured in the first-story shear-wall. As

observed from our experimental and analytical investigations, the global tension/compression couple triggers this typical failure mechanism by creating pure axial tension in shear-walls, which may cause longitudinal tension cracks and sudden tensile loading to the wall reinforcements. These observations provide convincing field evidence that brittleness of reinforced concrete walls caused by under-reinforcement cannot be ignored when designing for seismic loads.

Acknowledgements

We would like to thank to two anonymous reviewers for their comments and suggestions. Funding for the experimental program provided by the Scientific and Technical Research Council of Turkey (INTAG 561) is also gratefully acknowledged. Any opinions, findings, and conclusions or recommendations expressed in this material are those of the authors, and do not necessarily reflect the views of the Scientific and Technical Research Council of Turkey or the California Geological Survey.

References

ACI 318-2002 (2002), "Building code requirements for reinforced concrete and commentary", ACI, Detroit, Michigan, pp.119, 234-236.

ACI 318-83 (1983), "Building code requirements for reinforced concrete and commentary", ACI, Detroit, Michigan, pp.111.

Balkaya, C. and Kalkan, E. (2003), "Estimation of fundamental periods of shear-wall dominant building structures", *Earthq. Eng. Struct. Dyn.*, **32**, 985-998.

Balkaya, C. and Kalkan, E. (2003), "Nonlinear seismic response evaluation of tunnel form building structures", *Comput. Struct.*, **81**, 153-165.

Balkaya, C. and Kalkan, E. (2004), "Seismic vulnerability, behavior and design of tunnel form buildings", *Eng. Struct.*, **26**(14), 2081-2099.

Balkaya, C. and Kalkan, E. (2004), "Three-dimensional effects on openings of laterally loaded pierced shear-walls", *J. Struct. Eng.*, ASCE, **130**(10), 1506-1514.

Ghrib, F. and Mamedov, H. (2004), "Period formulas of shear-wall buildings with flexible bases", *Earthq. Eng. Struct. Dyn.*, **33**, 295-314.

Hordijk, D.A. (1991), *Local Approach to Fatigue of Concrete*, PhD thesis, Delft University of Technology.

International Conference of Building Officials (ICBO) (1997), Uniform Building Code (UBC), Whittier, Calif.

International Conference of Building Officials (ICBO) (2000), International Building Code (IBC), Whittier, Calif.

Kalkan, E. and Yuksel, B. (2007), "Pros and Cons of RC tunnel form (Box-type) buildings", *The Structural Design of Tall and Special Buildings*, **16**(2).

Lee, L., Chang, K. and Chun, Y. (2004), "Experimental formula for the fundamental period of RC buildings with shear-wall dominant systems", *Struct. Design of Tall Buildings,* **9**(4), 295-307.

Ministry of Public Work and Settlement. Turkish Seismic Code (TSC) - Specifications for the Structures to be Built in Disaster Regions, Ankara, 1998.

Popovics, S. (1973), "A numerical approach to the complete stress-strain curve for concrete", *Cem. Concr. Res.*, **3**(5), 583-599.

Thorenfeldt, E., Tomaszewicz, A. and Jensen, J.J. (1987), "Mechanical properties of high strength concrete and application in deisng", Proc., Symposium "Utilization of High Strength Concrete," Stavanger, Norway, June, Tapit, Trondheim, 149-159.

TNO DIANA, version 8.1, TNO Building Construction and Research, Delft, The Netherlands, 2004.

Wood, S.L. (1989), "Minimum tensile reinforcement requirements in walls", *ACI Struct. J.*, **86**(4).

Wood, S.L. (1990), "Shear strength of low-rise reinforced concrete walls", *ACI Struct. J.*, **87**(1).
Wood, S.L., Stark, R. and Greer, S.A. (1991), "Collapse of eight-story RC building during 1985 Chile earthquake", *J. Struct. Eng.*, ASCE, **117**(2), 600-619.
Yuksel, S.B. (2003), "Experimental investigation of the seismic behavior of panel buildings", PhD Dissertation, Middle East Technical University, Ankara.

Notation

A, A_g : concrete cross-section area (for SP1 and SP2, it is H-shape wall section)
A_{cv} : effective area of concrete cross-section (for SP1 and SP2, it is H-shape wall section)
f_c' : concrete compression strength (in psi)
f_y : reinforcement yield stress
h_w : wall height
l_w : total wall length
P : axial load
R : response modification factor in TSC 1998
V_{max} : maximum lateral force resisted by the wall
v_{max} : maximum average shear-stress
v_n : nominal shear strength of the wall (defined by ACI 318-83)
α_c : relative contribution of concrete strength to wall strength
ρ_n : reinforcement ratio of distributed web reinforcement (ACI 318-83)
ρ_t : total reinforcement ratio